AMERICAN METEOROLOGICAL SOCIETY

Bulletin of the American Meteorological Society

EARLY ONLINE RELEASE

This is a preliminary PDF of the author-produced manuscript that has been peer-reviewed and accepted for publication. Since it is being posted so soon after acceptance, it has not yet been copyedited, formatted, or processed by AMS Publications. This preliminary version of the manuscript may be downloaded, distributed, and cited, but please be aware that there will be visual differences and possibly some content differences between this version and the final published version.

The DOI for this manuscript is doi: 10.1175/BAMS-D-14-00017.1

The final published version of this manuscript will replace the preliminary version at the above DOI once it is available.

Global view of real-time TRMM Multi-satellite Precipitation Analysis: implication to its successor Global Precipitation Measurement mission

Bin Yong[1*], Die Liu[1], Jonathan J. Gourley[2], Yudong Tian[3,4], George J. Huffman[5], Liliang Ren[1], Yang Hong[6,7*]

1. State Key Laboratory of Hydrology-Water Resources and Hydraulic Engineering, Hohai University, Nanjing 210098, China;
2. NOAA/National Severe Storms Laboratory, Norman, OK 73072, USA;
3. Hydrological Sciences Branch, NASA Goddard Space Flight Center, Greenbelt, MD 20771, USA;
4. Earth System Science Interdisciplinary Center, University of Maryland, College Park, MD20740, USA;
5. Mesoscale Atmospheric Processes Laboratory, NASA Goddard Space Flight Center, Greenbelt, MD20771, USA;
6. Advanced Radar Research Center, National Weather Center, Norman, OK 73072, USA;
7. School of Civil Engineering and Environmental Sciences, University of Oklahoma, Norman, OK 73019, USA.

Manuscript for the ***Bulletin of the American Meteorological Society***

Date: June 8, 2014

Corresponding authors and address:

Bin Yong and Yang Hong, Drs., Professors

No. 1 Xikang Road, State Key Laboratory of Hydrology-Water Resources and Hydraulic Engineering, Hohai University, Nanjing 210098, China.

Tel.: +86-25-83787052; Fax: +86-25-83786606.

E-mail: yongbin_hhu@126.com; yanghong@ou.edu

Capsule

The global error characteristics of Tropical Rainfall Measuring Mission (TRMM)-based "best-effort" real-time precipitation estimates and their regional and seasonal variations are benchmarked as a baseline for its successor Global Precipitation Measurement (GPM) mission.

Abstract

Accurate estimation of high-resolution precipitation on the global scale is extremely challenging. The operational Tropical Rainfall Measuring Mission (TRMM) Multi-satellite Precipitation Analysis (TMPA) has created over 16 years of high-resolution quantitative precipitation estimation (QPE), and has built the foundation for improved measurements in the upcoming Global Precipitation Measurement (GPM) mission. TMPA is intended to produce the "best-effort" estimates of quasi-global precipitation from almost all available satellite-borne precipitation-related sensors by consistently calibrating them with the high-quality measurements from the core instrument platform aboard TRMM. Recently, the TMPA system has been upgraded to Version-7 to take advantage of newer and better sources of satellite inputs than Version-6, and has attracted a large user base. A key product from TMPA is the near-real-time product (TMPA-RT), as its timeliness is particularly appealing for time-sensitive applications such as flood and landslide monitoring. TMPA-RT's error characteristics on a global scale have yet to be extensively quantified and understood. In this study, efforts are focused on a systematic evaluation of four sets of mainstream TMPA-RT estimates on the global scale. Our analysis indicates that the latest Version-7 TMPA-RT with the monthly climatological calibration had the lowest daily systematic biases of approximately 9% over land and -11% over ocean (relative to the gauge-adjusted research product). However, there still exists some unresolved issues in mountainous areas (especially Tibetan Plateau), high-latitude belts, and for estimating extreme rainfall rates with high variability at small scales. These global error characteristics and their regional and seasonal variations revealed in this paper are expected to serve as the benchmark for the upcoming GPM mission.

Global view of real-time TRMM Multi-satellite Precipitation Analysis: implication to its successor Global Precipitation Measurement mission

1 Introduction

Precipitation is a key component of the global water cycle (Allen and Ingram, 2002; Wu et al., 2013). The measurement of precipitation at global scale is therefore crucial for a comprehensive understanding of the climate, weather, hydrology, and ecological systems (Wentz et al., 2007; Bunde et al., 2013; Liu et al., 2013). However, precisely measuring precipitation in many regions of the Earth is still a challenging task owing to the high spatial variability of precipitation and the sparseness of the surface-based observing networks (Ebert et al., 2007; Min et al., 2011). Especially over oceans, deserts, and mountainous areas, it is mostly infeasible to fully monitor precipitation with conventional rain gauge networks or weather radars. Satellite-based remote sensing can offer an alternative source of precipitation information for vast areas of the Earth's surface and has presently become the only practical way to measure precipitation on a global basis (Tian and Peters-Lidard, 2010; Kidd et al., 2012).

An important new program for global precipitation estimation is the Global Precipitation Measurement (GPM) mission lead by the National Aeronautics and Space Administration (NASA) and the Japan Aerospace Exploration Agency (JAXA) (Kidd and Huffman, 2011). The GPM is composed of one Core Observatory satellite and approximately eight constellation satellites. The GPM Core Observatory was successfully launched by the H-IIA launch vehicle No. 23 at 1:07 p.m. EST on February 28, 2014 (www.jaxa.jp/countdown/f23). This core satellite carries a Dual-frequency Precipitation Radar (DPR; the Ku-band at 13.6 GHz and Ka-band at 35.5 GHz) and a multi-channel

GPM Microwave Imager (GMI; frequency range between 10 and 183 GHz), which will be used together to develop a new calibration standard for the other microwave radiometers on the constellation satellites (Tapiador et al., 2012; Hou et al., 2014). In addition to these passive microwave sensors aboard low-Earth orbiting (LEO) satellite, GPM will utilize infrared measurements from geostationary satellites, yielding precipitation estimates around the globe at 0.1-deg, 30-min resolution. In general, the Core Observatory will help to observe worldwide precipitation (rain and snowfall) rates several times per day. Therefore, it is anticipated that GPM will improve climate, weather, and hydrological predictions through more accurate and more frequent precipitation measurements from space, aiming for a 3-hour interval for the LEO microwave observations. This should help meteorologists to better understand how Earth's hydrological cycle works.

As a prelude to GPM, the current operational Tropical Rainfall Measuring Mission (TRMM) Multi-satellite Precipitation Analysis (TMPA) system produces estimates of quasi-global rainfall (50°N–50°S) at relatively fine resolution (0.25°×0.25°, 3 hr) (Huffman et al., 2007; Yong et al., 2013). The TMPA is computed twice—first in near-real-time (TMPA-RT; 6-9 hours after observation time), and then again in post-real-time (TMPA-P; two months latency) for research purposes. These two types of TMPA standard products have been widely utilized in a variety of research and operational applications (Vallarini and Krajewski, 2007; Habib et al., 2009; Kidd et al., 2009; Tobin and Bennett, 2010; Behrangi et al., 2011; Khan et al., 2011; Romilly and Gebremichael, 2011; Habib et al., 2012; Wu et al., 2012; among many others). Prior studies indicate that the TMPA-RT estimates are less accurate than TMPA-P due to the lack of month-to-month gauge adjustments and high-quality TCI (TRMM Combined Instrument) calibration in the data processing algorithm (Su et al., 2008; Stisen and Sandholt, 2010; Yong et al., 2010; Bitew and Gebremichael, 2011). However, it is the near-real-time availability that makes TMPA-RT attractive for real-time hydrological forecasting and natural

93 hazard warning at local, regional, and even global scale (e.g., Hossain and Lettenmaier, 2006; Hong et
94 al., 2007; Gourley et al., 2013).

95 During the past decade, the TMPA real-time system has undergone three major upgrades
96 (corresponding to Versions -5, -6, and -7) because of the new sensors and upgraded algorithms (refer
97 to Yong et al., 2010 and Yong et al., 2012 for a detailed description). As one of the most important
98 algorithmic upgrades, a climatological calibration algorithm (CCA) was applied in TMPA's real-time
99 estimates from 1 October 2008 in Version-6, utilizing climatological gauge information to effectively
100 reduce systematic biases, while maintaining the near-real-time availability. For this monthly
101 calibration procedure, the developers first determined a local histogram matching of TMI (TRMM
102 Microwave Imager) to TCI, computed from 14 years of coincident data (in Version-7) to establish the
103 climatology for each calendar month. Then, a monthly climatological calibration of TCI to 3B43
104 (another TRMM product computed at monthly time intervals) is calculated as a simple ratio on a 1° ×
105 1° grid. The calibration factor is aggregated to an overlapping 3° × 3° boxcar template using 14 years
106 of data. Finally, the TMI-TCI and TCI-3B43 calibrations are applied sequentially to the preliminary
107 real-time products to create the calibrated TMPA-RT estimates.

108 The CCA is the primary upgrade from Version-5 to Version-6. Furthermore, this new
109 calibration has been used in the current Version-7, and a similar approach will carry over to the real-
110 time runs of the Integrated Multi-satellitE Retrievals for GPM (IMERG) algorithm. Version-7 also
111 introduced some newer passive microwave (PMW) and infrared (IR) sensors relative to Version-6,
112 mainly including the Special Sensor Microwave Imager/Sounder (SSMIS) F16-17, Microwave
113 Humidity Sounder (MHS) (N18 and N19), Meteorological Operational satellite programme (MetOp),
114 and the 0.07° Gridsat-B1 infrared data (http://trmm.gsfc.nasa.gov/).

115 As the GPM era is now upon us, studies will focus on the impact of the contemporary

116 measurements as well as continued algorithm development. Therefore, it seems timely for this paper
117 to provide some insights into the following questions frequently posed by the satellite QPE-hydrology
118 community: 1) How do the latest Version-7 TMPA-RT estimates perform at global scale (specifically
119 compared to Version-6)? and 2) Are the current TMPA precipitation algorithm concepts being used in
120 the new IMERG system ready for GPM?

121 Due to the lack of accurate and independent ground observations, we cannot directly quantify
122 the systematic errors of TMPA-RT estimates by surface validation data across the entire globe. To
123 provide a globally consistent evaluation, we first use the Version-7 TMPA-P product as the reference
124 for our comparisons in this study for the following reasons. First, it ingests the new Global
125 Precipitation Climatology Center (GPCC) (Rudolf et al., 1994) "full" gauge analysis, and hence
126 essentially reproduces the precipitation characteristics of the gridded GPCC dataset at monthly scale
127 in many land areas. Through these gauge adjustments, which also introduce rainfall patterns forced by
128 orography, the research product has been shown to successfully remove systematic biases of satellite
129 retrievals (Chen et al., 2013a; Chen et al., 2013b). Moreover, the TMPA developers attempted to
130 make the real-time data sets resemble TMPA-P as much as possible through the CCA calibration to
131 TCI. Therefore, the latest Version-7 TMPA-P research product gives us a suitable reference to
132 compare different TMPA real-time estimates on a global basis. The drawback is its lack of
133 independence from the real-time products being evaluated; the research product incorporated the same
134 remote-sensing measurements in the final products. In this paper, the "previous" uncalibrated and the
135 "new" climatologically calibrated TMPA-RT estimates for both Version-6 (RTV6_UC and RTV6_C
136 hereafter) and Version-7 (RTV7_UC and RTV7_C hereafter) are statistically investigated against
137 Version-7 TMPA-P (V7 hereafter) at the global scale. We also employed a gauge-based analysis of
138 daily precipitation produced by NOAA's Climate Prediction Center (CPC;

ftp://ftp.cpc.ncep.noaa.gov/precip/CPC_UNI_PRCP/) (Chen et al., 2008; Xie et al., 2010) to further evaluate the TMPA-RT precipitation products over four densely gauged regions. We selected an overlapping timespan of these six available data sets, three complete years from July 2008 to June 2011.

2 Results and Discussions

2.1 Global view of systematic biases in TMPA-RT estimates

A global map of mean daily precipitation difference between the four TMPA real-time estimates (RTV6_UC, RTV6_C, RTV7_UC, and RTV7_C) and the V7 post-real-time research product gives a clear indication of where the data sets are performing better or worse. In general, RTV6_C and RTV7_C have lower relative biases than their corresponding uncalibrated estimates (Fig. 1). Most notably along the Western Pacific Ocean Convergence Zone (near 10°S) extending over the Philippines, Indonesia, and Malaysian Islands, southeastern China, and into the Indian Ocean, the CCA calibration significantly elevated the uncalibrated TMPA-RT estimates so as to effectively reduce their substantial negative biases. Similar patterns were also found in the narrow Inter-Tropical Convergence Zone across the Atlantic Ocean extending toward Central America. Likewise, such upward adjustments also alleviate the systematic underestimation along most coastlines (e.g., the western coast of India and the eastern coast of American Continent) and over inland water bodies (e.g., the Great Lakes).

Insert Figure 1 here

From Fig. 2, it can be seen that these extreme negative biases primarily occurred in the boreal warm season (June, July, and August – JJA). The patterns of underestimation by the uncalibrated products seem to correspond to climatological maxima of tropical rain features and the migration of

161 the Asian Summer Monsoon. On the other hand, there is an apparent overestimation with the
162 uncalibrated RTV6_UC and RTV7_UC datasets in central Africa (an area just to the west of Lake
163 Victoria, see Figs.1a and 1c), especially during the rainy seasons (refer to plots of 'MAM' and 'SON'
164 in Fig. 2). Over this region, significant reductions resulted following the CCA calibration, thereby
165 reducing the most significant positive biases for the uncalibrated TMPA-RT products.

166 **Insert Figure 2 here**

167 Over land, almost all regions exhibit strong seasonality of bias. For example, Europe has much
168 larger negative biases in winter due to erroneous retrievals of snow events during the cold season
169 (Yong et al., 2013). Over the eastern continental United States (CONUS), the negative biases with the
170 RTV6_UC and RTV7_UC estimates were also likely the result of snow events. A positive bias
171 appears in the Great Plains of the US presumably due to overestimation by the PMW-based land
172 algorithms for strong convective events during the warm season (Tian et al., 2009; Gourley et al.,
173 2010). Inter-comparing the TMPA-RT estimates before and after climatological calibration, one can
174 see that the CCA substantially improved these seasonal errors and biases for both versions (Fig. 2).

175 Many of the global error features in TMPA-RT estimates can be related to the overpass
176 frequency and retrieval characteristics of the PMW and IR sensors incorporated. Two types of PMW
177 sensors are currently available for TMPA, namely, conical-scanning imagers including TMI, AMSR,
178 SSMI, and SSMIS, and cross-track-scanning sounders including AMSU and MHS. Generally, the
179 imagers have better performance than the sounders (Lin and Hou, 2008; Tang et al., 2014), and TMPA
180 Version-7 system is using more imager overpasses than Version-6 on the global scale (see Figs. 3e
181 and 3f). [Note that the TMPA selects imager data over sounders when both are available in a gridbox
182 at a particular 3-hour time.] This is an improvement that takes advantage of more and better data
183 sources for producing merged Version-7 TMPA estimates. In addition, the proportion of

184 Geostationary Infrared-based retrievals (geo-IR) is reduced when compared to Version-6 (Figs. 3g and
185 3h). However the Tibetan Plateau is an exception. Over this region, the usage of geo-IR data with poor
186 correlation to precipitation is more frequent than the previous version (its scanning proportion
187 accounting for over 70% of total scans), likely due to more stringent quality control of the PMW
188 overpasses as they are unreliable over the snow cover and complex terrain in the Tibetan Plateau.
189 Therefore, the Geo-IR data is less certain given it is calibrated by the deficient PMW over this region.
190 On the other hand, geo-IR data themselves are not necessary more reliable, because of many
191 orographic rain events lacking the strong convective signatures for geo-IR detection. Therefore the
192 choice of geo-IR or PMW data sources over this area is equally challenging, and the fact that Version-
193 7 utilizes more geo-IR data than Version-6 is just a reflection of the large uncertainties in our
194 knowledge for this area (Tian and Peters-Lidard, 2010).

195 It is worth noting that the issues were not readily resolvable by calibrating to rain gauges.
196 Relative to the uncalibrated RTV7_UC, the calibrated RTV7_C has a dramatic overestimation in the
197 Tibetan Plateau (Fig. 1d). Such a significant discrepancy before and after climatological calibration
198 should be attributed to the CCA algorithm. Because of high elevation, complex terrain, severe weather,
199 and general inaccessibility, direct meteorological observations employed in the improved GPCC rain
200 gauge analyses do not exist over large portions of the Tibetan Plateau, especially in the mid-western
201 part of the plateau. Hence, the GPCC values used in the CCA calibration over the Tibetan Plateau
202 were mainly determined by the gridded interpolation results of its surrounding areas (e.g., India,
203 southeast Asia, and southeastern China). Over these surrounding regions extending to the western
204 Pacific Ocean and Indian Ocean, the upward adjustments of the CCA calibration evidently elevated
205 the RTV7_UC estimates at the large scale, but meanwhile unfavorably increased the original positive
206 biases over the Tibetan Plateau, particularly during the warm season (Figs. 2g and 2h). The tendency

to raise precipitation amounts seems to be more significant in Version-7 than that in Version-6 (Figs. 2e-2h), which could explain the larger positive biases in RTV7_C relative to RTV6_C (Figs. 1b and 1d). This is an indication of the large uncertainties in the gauge data as well. A similar phenomenon can also be found in the Tianshan Mountains north of the Himalayas and the Cordillera Mountains in the western coastal mountains of South America. From this global analysis, we have shown that the current Version-7 TMPA-RT data still have much uncertainty in high mountainous areas, especially at the Earth's "third pole".

Insert Figure 3 here

2.2 Improvement for both land and ocean

The density-colored scatterplots displayed in Fig. 4 give additional analyses of how the CCA calibration works for two different TMPA versions over the whole domain, broken into land and ocean areas. In general, we can see that the scatterplots of calibrated TMPA-RT (bottom diagrams) have higher Pearson linear correlation coefficient (CC) and lower root mean squared error (RMSE) and the points are clustered more closely to the 1:1 line than for the uncalibrated estimates (top). The uncalibrated TMPA-RT products substantially underestimate precipitation over both land and ocean, while the CCA calibration effectively reduced such systematic negative biases. Over land, all the statistical indices indicate that the RTV7_C outperformed RTV6_C with higher correlation and lower error and bias. Over oceanic regions, the mean error (ME) and relative bias (BIAS) of RTV7_C are slightly larger than those of RTV6_C. But it cannot be considered that the latter is superior to the former, since the overall bias is the average results offset by opposing signs in different regions. The CC and RMSE are informative here, and indeed show better performance by RTV7_C. Overall, our evaluation indicates that the RTV7_C provides the best daily precipitation estimates and its systematic bias is 8.89% for land and -10.83% for ocean (benchmarked by V7), respectively. RTV7_C has better

CC and lower RMSE over oceanic regions than over land. This is likely due to superior performance of the PMW algorithms over ocean.

Insert Figure 4 here

2.3 Latitudinal profile of TMPA estimates

Figure 5 depicts the latitudinal distribution of the annual mean precipitation of the four TMPA-RT estimates against V7 over both land and ocean. From this latitudinal profile, one tends to see relatively larger and more complicated oscillations over land areas than ocean, particularly in the Northern Hemisphere. This is mainly due to the small-scale variability of continental precipitation associated with orography. Over land, the profile curves of calibrated TMPA-RT estimates are rather close to that of V7 in the deep tropics, roughly between 25°N and 18°S (Fig. 5a). The overestimation of RTV6_C and RTV7_C (corresponding to Figs. 4c and 4d) mostly appears from 25°N to 50°N in the Northern Hemisphere. Furthermore, RTV7_C has significant overestimation at mid-latitudes between 25°N and 35°N, even worse than RTV6_C. This is because of the aforementioned retrieval and calibration issues arising from the updated Version-7 system primarily over the Tibetan Plateau.

At latitudes beyond 35°N, the RTV6_C seemed to excessively elevate the uncalibrated TMPA-RT estimates (e.g., Europe, Middle East, and eastern United States, refer to Figs. 1a and 1b), while a relatively better performance was found for RTV7_C. Additionally, we note that the most significant underestimation with RTV6_UC and RTV7_UC occurred from 15°N to 30°N. At this latitude band, the CCA calibration works best and effectively mitigates the systematic negative biases particularly in southeastern China, southeast Asia, and India (see Fig. 1). This is mainly because of the dense ground observing networks distributed over these regions, hence offering robust gauge adjustments using the GPCC full analysis in the CCA calibration scheme. Relative to land, the latitudinal profile curves over

252 the oceans look more stable and smoother (Fig. 5b). Maximum over-ocean rainfall is situated at 7°N,
253 while the land maximum is at about 3°S. Similar to the patterns in Fig. 5a, the systematic
254 underestimation with uncalibrated TMPA-RT were also alleviated after the CCA calibration over the
255 ocean, especially for the latitude band 20°N-S (Fig. 5b). But, in general, the calibrated TMPA-RT
256 estimates still contain negative biases as compared to V7.

257 **Insert Figure 5 here**

258 2.4 Evaluation of TMPA-RT estimates over the globe

259 The daily statistics of the four TMPA-RT datasets against the gauge-adjusted V7 product are
260 summarized in Table 1 for land, ocean, and global domains in the latitude band 50° N-S for different
261 seasons. First, all statistical indices with the Version-6 TMPA-RT are substantially improved in most
262 cases. However, the boreal winter season is different, during which slightly lower CC and higher
263 RMSE values were found for all areas. In terms of ME and BIAS, precipitation over land seems to be
264 elevated a little more for both the autumn and winter seasons. For Version-6, most of the changes in
265 the four representative statistical indices point to the success in the CCA calibration scheme. As for
266 Version-7, the RTV7_C estimates apparently outperformed RTV7_UC according to almost all
267 statistics, except for a little larger ME and BIAS values over land in summer. This arises because of
268 the retrieval issues and lack of effective CCA calibration due to sparse rain gauges over the
269 Himalayan region. Overall, the near-unanimous improvement after the CCA calibration over both land
270 and ocean further confirms our spatial analysis results as presented in the prior sections. The
271 systematic errors and biases in the original uncalibrated TMPA-RT were generally alleviated after the
272 CCA was applied.

273 **Insert Table 1 here**

2.5 Gauge-based validation of TMPA-RT estimates over four representative regions

Up to now, the TMPA-RT estimates were evaluated over the globe using the V7 post-real-time research product as reference. The primary advantage was the availability of matched data at each grid point over land and ocean. However, despite the research product being heavily influenced by the GPCC gauges, it uses the same remote-sensing data in its estimation scheme as the TMPA-RT. Further, the CCA bias adjustment to the RT products is based on the monthly GPCC gauge accumulations. So, the evaluation was not performed with independent datasets. In this section, we adopted the CPC unified gauge-based analysis (Chen et al., 2008; Xie et al., 2010) as the reference to further evaluate the global precipitation products over land. The CPC precipitation data set (at a daily, 0.5°×0.5° latitude-longitude resolution) is computed by interpolating gauge observations from over 30,000 stations through the optimal interpolation (OI) algorithm of Xie et al. (2007). The degree to which the CPC data set is different from what Huffman et al. (2010) used for the gauge analysis in TMPA-P estimates and CCA calibration is not known. However, the CPC-based analysis was performed at daily scale which provides independent information about the random errors with the TMPA-RT products. Our quantitative validation was performed over the United States, East Asia, Europe, and Australia (see Fig. 6). The four regions were chosen because of their relatively dense gauge networks that can offer reliable ground verification for the TMPA-RT estimates. Furthermore, these regions cover a wide range of climate regimes and land surface characteristics (Ebert et al., 2007).

Insert Figure 6 here

In this study, the four TMPA-RT datasets were resampled to 0.5°×0.5° resolution

296 corresponding to the spatial scale of the CPC gauge analysis. In order to reduce the uncertainty in the
297 validation results, we only selected grid boxes that contained at least one gauge to compute the daily
298 statistics between the TMPA-RT estimates and the CPC gauge analysis.

299 Table 2 summarizes the seasonal statistics before and after the CCA calibration for the four
300 densely gauged regions. With respect to the indices of CC, ME, and BIAS, the CCA exhibits an
301 effective improvement over its respective, uncalibrated versions for all the validation regions. Taking
302 Version-7 as an example, the CCA increased the correlation between TMPA-RT and the CPC gauge
303 observations (except in Australia during winter) and significantly reduced the ME and BIAS values.
304 These results are consistent with our global evaluation results in 2.4. But, we note that the daily
305 RMSE became worse after the calibration in most cases, such as in East Asia and Australia, which are
306 contrary to the results in Table 1. This implies that the CCA made the real-time estimates statistically
307 closer to the research product, but not to the CPC gauge observations. This is likely due to the sparser
308 gauge data used in CCA in these regions and the scale differences over which the CCA was applied
309 relative to the daily accumulations. Since the monthly climatological calibrators in the CCA seemed to
310 amplify the dynamic range of daily precipitation, the daily RMSE still increased despite the decreased
311 systematic bias. The basin-scale assessment of Yong et al. (2013) shows the CCA tends to improve on
312 the error and bias by primarily altering the precipitation estimates at higher rain rates. The primary
313 concern from these results is that the employment of the historical gauge data and the smooth-fill
314 scheme in the CCA monthly bias correction could homogenize the highly variable local rainstorm
315 characteristics. This characteristic might be unfavorable to heavy rainfall-related flood forecasting and
316 landslide warning. Therefore, it is important to continue providing the uncalibrated real-time
317 precipitation as an additional field in the forthcoming IMERG products for GPM users, as is being
318 done in current TRMM Version-7.

Insert Table 2 here

3 Summary and Outlook

A systematic evaluation of the recent four TMPA real-time data sets against the V7 research product from July 2008 to June 2011 shows that the latest Version-7 TMPA-RT with climatological calibration has lower systematic biases and smaller random errors over both land and ocean relative to the other three versions of TMPA-RT estimates. From a global perspective, the Version-7 TMPA calibration concepts could be considered as essentially ready for new measurements coming in the GPM era. However, both analyses indicate the current TRMM-era retrievals still have room for improvement. The CPC gauge-based analysis over four continental sub-regions showed higher RMSE values following application of the climatological calibration. While removing systematic bias at the monthly scales, the calibration scheme may have introduced deleterious effects on daily rainfall accumulations. This characteristic may have negative impacts for estimating heavy rainfall with high local variability at small scales. Another problem area was detected in high mountainous regions (e.g. the Himalayas) and high latitudes. The retrieval algorithms suffer from the effect of persistent snow cover, and are generally less accurate in estimating falling snow. This highlights a word of caution when using the Version-7 TMPA-RT estimates for monitoring precipitation over these specific zones and for highly variable extreme rainfall amounts. Although the newly introduced sensors and upgraded calibration algorithms have undoubtedly improved the TMPA's accuracy, some challenging issues in satellite retrieval processes will continue to remain open for the satellite QPE-hydrology community, providing impetus for more research and development.

The GPM is a unique and complex program. The successful integration of the GPM Core Observatory instruments will substantially change the sensor composition and inter-calibration scheme available for multi-satellite estimation. Relative to TRMM, GPM is designed to make more

342 accurate and frequent observations of global rainfall, especially over middle and high latitudes (Hou et
343 al., 2014). Now, the GPM project is adopting the new Goddard Profiling Algorithm (a multi-channel
344 physical approach which has been named GPROF2014) to unify all of the available microwave
345 observations over the latitude band 68° N-S so as to provide, for the first time, adequate sampling and
346 accuracy of precipitation (both rain and snow) as calibrators beyond TRMM's 37° N-S band. During
347 the satellite check-out, most activities are focused on the GPM-era algorithm development and
348 validation with respect to the recent updates. One of the immediate tasks at hand is to complete the
349 current testing and validation of the dual-frequency radar algorithm to derive characteristics of the rain
350 drop spectra. Other important tasks for obtaining global precipitation estimates include extending
351 quantitative precipitation estimation to higher latitudes, and higher elevations and further improving
352 the retrievals during winter months. With respect to the current monitoring skills, it is almost certain
353 that regions characterized by complex terrain and snowy/ice cover will still be problematic for the
354 day-1 multi-satellite retrieval in GPM.

355 In summary, we expected that the global analysis of TRMM-based precipitation estimates
356 reported here can give the satellite precipitation users a better understanding of the error features
357 associated with currently available TMPA real-time precipitation estimates from a broader perspective.
358 These results will better guide those users who are taking advantage of these satellite-based
359 quantitative precipitation data to accommodate their various research and operational applications.

Acknowledgements

This work was financially supported by National Science Foundation of China (51379056). The TMPA data used in this study were provided by the NASA/Goddard Space Flight Center's Mesoscale Atmospheric Processes laboratory and PPS, which develop and compute the TMPA as a contribution to TRMM. The authors thank three anonymous reviewers who helped to improve the earlier version of this paper.

References

Allen, M. R., and W. J. Ingram, 2002: Constraints on future changes in climate and the hydrologic cycle. *Nature*, **419**, 224-232.

Behrangi, A., B. Khakbaz, T. C. Jaw, A. Aghakouchak, K. Hsu, and S. Sorooshian, 2011: Hydrologic evaluation of satellite precipitation products over a mid-size basin. *J. Hydrol.*, **397**, 225-237.

Bitew, M. M., and M. Gebremichael, 2011: Evaluation of satellite rainfall products through hydrologic simulation in a fully distributed hydrologic model. *Water Resour. Res.*, **47**, W06526, doi: 10.1029/2010WR009917.

Bunde, A., U. Buntgen, J. Ludescher, J. Luterbacher, and H. Storch, 2013: Is there memory in precipitation? *Nature Clim. Change*, **3**, 174-175.

Chen, M., W. Shi, P. Xie, V. B. S. Silva, V. E. Kousky, R. W. Higgins, and J. E. Janowiak, 2008: Assessing objective techniques for gauge-based analyses of global daily precipitation. *J. Geophys. Res.*, **113**, D04110, doi: 10.1029/2007JD009132.

Chen, S., et al, 2013a: Similarity and Difference of the two Successive V6 and V7 TRMM Multi-satellite Precipitation Analysis (TMPA) Performance over China. *J Geophys Res.*, **118**, 13,060-13,074.

Chen, S., et al, 2013b: Evaluation of the Successive V6 and V7 TRMM Multi-satellite Precipitation Analysis Over the Continental United States. *Water Resour. Res.*, **49**, 8174-8186.

Ebert, E. E., J. E. Janowiak, and C. Kidd, 2007: Comparison of near-real-time precipitation estimates from satellite observations and numerical models. *Bull Am. Meteorol. Soc.*, **88**, 47-64.

Gourley, J. J., Y. Hong, Z. L. Flamig, L. Li, and J. Wang, 2010: Intercomparison of rainfall estimates from radar, satellite, gauge, and combinations for a season of record rainfall. *J Appl. Meteorol. Climatol.*, **49**, 437-452.

Gourley, J. J., et al, 2013: A Unified Flash Flood Database over the US. *Bull Am. Meteorol. Soc.*, **94**, 799-805.

Habib, E., M. ElSaadani, and A. T. Haile, 2012: Climatology-Focused Evaluation of CMORPH and TMPA Satellite Rainfall Products over the Nile Basin. *J. Appl. Meteorol. Climatol.*, **51**, 2105-2121.

Habib, E., A. Henschke, and R. F. Adler, 2009: Evaluation of TMPA satellite-based research and real-time rainfall estimates during six tropical-related heavy rainfall events over Louisiana, USA. *Atmos. Res.*, **94**, 373-388.

Hong, Y., R. F. Adler, and G. Huffman, 2007: An experimental global prediction system for rainfall-triggered landslides using satellite remote sensing and geospatial datasets. *IEEE Trans. Geosci. Rem. Sens.*, **45**, 1671-1680.

Hossain, F., and D. P. Lettenmaier, 2006: Flood prediction in the future: Recognizing hydrologic

issues in anticipation of the Global Precipitation Measurement mission. *Water Resour. Res.*, **42**, W11301, doi: 10.1029/2006WR005202.

Hou, A. Y., R. K. Kakar, S. Neeck, A. A. Azarbarzin, C. D. Kummerow, M. Kojima, R. Oki, K. Nakamura, and T. Iguchi, 2014: The Global Precipitation Measurement (GPM) Mission. *Bull Am. Meteorol. Soc.*, **in Press**, doi: 10.1175/BAMS-D-13-00164.1.

Huffman, G. J., R. F. Adler, D. T. Bolvin, G.Gu, E. J. Nelkin, K. P. Bowman, Y. Hong, E. F. Stocker, and D. B .Wolff, 2007: The TRMM Multisatellite Precipitation Analysis (TMPA): Quasi-global, multiyear, combined-sensor precipitation estimates at fine scales. *J. Hydrometeorol.*, **8**, 38-55.

Khan, S. I., Y. Hong, J. Wang, K. K. Yilmaz, J. J. Gourley, R. F. Adler, G. R. Brakenridge, F. Policell, S. Habib, and D. Irwin, 2011: Satellite remote sensing and hydrologic modeling for flood inundation mapping in Lake Victoria Basin: Implications for hydrologic prediction in ungauged basins. *IEEE Trans. Geosci. Rem. Sens.*, **49**, 85-95.

Kidd, C., V. Levizzani, J. Turk, and R. Ferraro, 2009: Satellite precipitation measurements for water resource monitoring. *J. Amer. Water Resour. Assoc.*, **45**, 567-579.

Kidd, C., and G. J. Huffman, 2011: Global precipitation measurement. *Meteorol. Appl.*, **18**, 334-353.

Kidd, C., P. Bauer, J. Turk, G. J. Huffman, R. Joyce, K. –L. Hsu, and D. Braithwaite, 2012: Intercomparison of high-resolution of precipitation products over Northwest Europe. *J.*

435 *Hydrometeorol.*, **13**, 67-83.

436

437 Lin., X., and A. Y. Hou, 2008: Evaluation of coincident passive microwave rainfall estimates using
438 TRMM PR and ground measurements as references. *J. Appl. Meteor.*, **47**, 3170-3187.

439

440 Liu, J., B. Wang, M. A. Cane, S. Y. Yim, and J. Y. Lee, 2013: Divergent global precipitation changes
441 induced by nature versus anthropogenic forcing. *Nature*, **493**, 656-659.

442

443 Min, S. K., X. Zhang, F. W. Zwiers, and G. C. Hegerl, 2011: Human contribution to more-intense
444 precipitation extremes. *Nature*, **470**, 378-381.

445

446 Romilly, T. G., and M. Gebremichael, 2011: Evaluation of satellite rainfall estimates over Ethiopian
447 river basins. *Hydrol. Earth Sys. Sci.*,**15**, 1505-1514.

448

449 Rudolf, B., H. Hauschild, W. Rueth, and U. Schneider, 1994: Terrestrial precipitation analysis:
450 Operational method and required density of point measurements. *Global precipitation and Climate*
451 *change*, **26**, 173-186.

452

453 Stisen, S., and I. Sandholt, 2010: Evaluation of remote-sensing-based rainfall products through
454 predictive capability in hydrological runoff modelling. *Hydrol. Processes*, **24**, 879-891.

455

456 Su, F., Y. Hong, and D. P. Lettenmaier, 2008: Evaluation of TRMM Multisatellite Precipitation
457 Analysis (TMPA) and its utility in hydrologic prediction in the La Plata Basin. *J. Hydrometeorol.*, **9**,

622-640.

Tang, L, Y. Tian, and X. Lin, 2014: Validation of precipitation retrievals from satellite-based passive microwave sensors, *J. Geophys. Res.*, **119**, doi:10.1002/2013JD020933.

Tapiador, F. J., et al., 2012: Global precipitatin measurement: Methods, datasets and applications. *Atmos. Res.*, **104–105**, 70-97.

Tian, Y., C. D. Peters-Lidard, J. B. Eylander, R. J. Joyce, G. J. Huffman, R. F. Adler, K. Hsu, F. J. Turk, M. Garcia, and J. Zeng, 2009: Component analysis of errors in satellite-based precipitation estimates. *J. Geophys. Res.*, **114**, D24101, doi: 10.1029/2009JD011949.

Tian, Y., and C. D. Peters-Lidard, 2010: A global map of uncertainties in satellite-based precipitation measurements. *Geophys. Res. Lett.*, **37**, L24407, doi: 10.1029/2010GL046008.

Tobin, K. J., and M. E. Bennett, 2010: Adjusting satellite precipitation data to facilitate hydrologic modeling. *J. Hydrometeorol*., **11**, 966-978.

Villarini, G., and W. F. Krajewski, 2007: Evaluation of the research version TMPA three-hourly 0.25× 0.25 rainfall estimates over Oklahoma. *Geophys. Res. Lett.*, **34**, L029147, doi: 10.1029/2006GL029147.

Wentz, F., L. Ricciardulli, K. Hilburn, and C. Mears, 2007: How much more rain will gobal warming

bring? *Science*, **317**, 233-235.

Wu, H., R. F. Adler, Y. Hong, Y. Tian, F. Policelli, 2012: Evaluation of global flood detection using satellite-based rainfall and a hydrologic model. *J. Hydrometeorol.*, **13**, 1268-1284.

Wu, P., N. Christidis, and P. Stott, 2013: Anthropogenic impact on Earth's hydrological cycle. *Nature Clim. Change*, **3**, 807-810.

Xie, P., A. Yatagai, M. Chen, T. Hayasaka, Y. Fukushima, C.Liu, and S. Yang, 2007: A Gauge-based analysis of daily precipitation over East Asia. *J. Hydrometeorol.*, **8**, 607-626.

Xie, P., M. Chen, and W. Shi, 2010: CPC unified gauge-based analysis of global daily precipitation. Preprints, *24th Conf. on Hydrology, Atlanta, GA*, Amer. Meteor. Soc., **2.3A**.

Yong, B., L.-L. Ren, Y. Hong, J.-H. Wang, J. J. Gourley, S.-H. Jiang, X. Chen, and W. Wang, 2010: Hydrologic evaluation of Multisatellite Precipitation Analysis standard precipitation products in basins beyond its inclined latitude band: A case study in Laohahe basin, China. *Water Resour. Res.*, **46**, W07542.

Yong, B., Y. Hong, L.-L. Ren, J. J. Gourley, G. J. Huffman, X. Chen, W. Wang, and S. I. Khan, 2012: Assessment of evolving TRMM-based multisatellite real-time precipitation estimation methods and their impacts on hydrologic precipitation in a high latitude basin. *J. Geophys. Res-Atmos.*, **117**, D09108, doi: 10.1029/2011JD017069.

Yong, B., L.-L. Ren, Y. Hong, J. J. Gourley, Y. Tian, G. J. Huffman, X. Chen, W. Wang, and Y. Wen, 2013: First evaluation of the climatological calibration algorithm in the real-time TMPA precipitation estimates over two basins at high and low latitudes, *Water Resour. Res.*, **49**, 2461-2472, doi: 10.1029/2009WR008965.

Figure Captions List

Figure 1. Global map of mean daily precipitation difference between (a) uncalibrated RTV6 data sets (RTV6_UC) and production V7, (b) calibrated RTV6 (RTV6_C) and production V7, (c) uncalibrated RTV7 (RTV7_C) and production V7, (d) calibrated RTV7 (RTV7_C) and production V7 for the three-year study period (from July 2008 to June 2011).

Figure 2. As in Fig. 1, but for seasonal variations: boreal (a-d) Spring (March-May), (e-h) Summer (June-August), (i-l) Autumn (September-November), and (m-p) Winter (December-February).

Figure 3. Global distribution of scan frequency of various microwave sensors introduced into the (left column) Version-6 and (right column) Version-7 TMPA real-time system: (a) and (b) No Observation; (c) and (d) Imagers; (e) and (f) Sounders; (g) and (h) IR.

Note: In the text, the scan frequency of a certain kind of sensors (SF_i) is defined as following:

$$SF_i = \frac{SC_i}{SC_{total}} \times 100\% \qquad (1)$$

where SC_i is the scan counts of a certain kind of sensors, SC_{total} is the total scan counts for all sensors.

Figure 4. Two-dimensional scatterplots of daily precipitation for (top) uncalibrated and (bottom) calibrated TMPA-RT against production V7 for (left two columns) land and (right two columns) ocean, corresponding to the maps in Fig. 1.

Note: The formulae and meaning of all statistical indices in each plot are described in more detail in Table 1 of Yong et al. (2010).

Figure 5. Latitudinal distribution of the annual mean precipitation of four TMPA-RT estimates (RTV6_UC, RTV6_C, RTV7_UC, RTV7_C) and production V7 over both (a) land and (b) ocean.

Figure 6. Number of gauge stations in a 0.5° × 0.5° latitude-longitude grid for the CPC unified gauge-based analysis over the global land areas (from July 2008 to June 2011). The four selected validation

531 regions (i.e., United States, East Asia, Europe, and Australia) are also shown.

532 **Table 1.** Seasonal statistics of comparing daily accumulations of uncalibrated and calibrated TMPA-RT estimates (i.e., RTV6_UC,
533 RTV7_UC, RTV6_C, and RTV7_C), taking daily V7 as the reference. Results are displayed for land, ocean, and global domains in
534 the latitude band 50°N–50°S during the study period July 2008-June 2011. Shading indicates better statistics in each UC/C pair.

Season	Item	CC				ME(mm/day)				RMSE(mm/day)				BIAS (%)			
		RTV6_UC	RTV6_C	RTV7_UC	RTV7_C	RTV6_UC	RTV6_C	RTV7_UC	RTV7_C	RTV6_UC	RTV6_C	RTV7_UC	RTV7_C	RTV6_UC	RTV6_C	RTV7_UC	RTV7_C
MAM	land	0.78	0.78	0.86	0.90	0.22	0.17	-0.31	0.14	5.54	5.42	4.06	3.69	9.36	7.33	-13.18	5.97
	ocean	0.86	0.87	0.94	0.95	-0.08	-0.07	-0.39	-0.24	4.71	4.66	3.30	3.04	-3.25	-2.69	-15.07	-9.29
	global	0.85	0.85	0.92	0.93	-0.004	-0.007	-0.37	-0.14	4.87	4.79	3.47	3.18	-0.18	-0.28	-15.60	-5.97
JJA	land	0.66	0.77	0.84	0.89	-0.57	0.16	-0.29	0.37	6.76	5.95	4.57	4.27	-21.67	6.30	-11.37	14.70
	ocean	0.78	0.87	0.94	0.95	-0.86	-0.28	-0.49	-0.32	6.29	4.78	3.46	3.20	-31.49	-10.27	-17.95	-11.98
	global	0.76	0.85	0.92	0.93	-0.78	-0.17	-0.43	-0.14	6.30	5.04	3.74	3.48	-30.71	-6.57	-17.31	-5.75
SON	land	0.72	0.78	0.85	0.89	-0.02	0.16	-0.20	0.11	5.95	5.33	4.19	3.63	-1.04	6.92	-8.85	4.99
	ocean	0.83	0.88	0.95	0.95	-0.47	-0.21	-0.46	-0.25	5.47	4.64	3.42	3.08	-17.48	-7.80	-17.06	-9.18
	global	0.81	0.86	0.92	0.94	-0.36	-0.12	-0.39	-0.15	5.51	4.76	3.60	3.20	-14.68	-4.81	-16.10	-6.34
DJF	land	0.78	0.77	0.86	0.89	-0.05	0.30	-0.52	0.13	5.47	5.92	4.27	3.92	-2.05	12.22	-21.40	5.45
	ocean	0.88	0.87	0.94	0.95	-0.19	-0.16	-0.40	-0.31	4.79	4.87	3.49	3.29	-7.03	-5.88	-14.87	-11.29
	global	0.86	0.85	0.92	0.93	-0.15	-0.04	-0.43	-0.19	4.91	5.10	3.67	3.43	-6.18	-1.69	-17.39	-7.69
All Seasons	land	0.74	0.79	0.86	0.90	-0.11	0.19	-0.33	0.19	5.76	5.49	4.16	3.79	-5.01	9.13	-15.30	8.86
	ocean	0.84	0.87	0.94	0.95	-0.40	-0.18	-0.43	-0.28	5.25	4.70	3.40	3.14	-15.60	-6.88	-16.96	-10.81
	global	0.81	0.85	0.92	0.93	-0.25	-0.12	-0.42	-0.18	5.28	4.92	3.61	3.30	-13.48	-3.42	-16.92	-6.62

535 **Table 2.** Seasonal statistics of comparing daily accumulations of uncalibrated and calibrated TMPA-RT estimates (i.e., RTV6_UC,
536 RTV7_UC, RTV6_C, and RTV7_C), taking daily CPC estimates as the reference. Results are displayed for four densely gauged
537 regions (i.e., United States, East Asia, Europe, and Australia) during the study period July 2008-June 2011. Shading indicates better
538 statistics in each UC/C pair.

539

Season	Item	CC				ME(mm/day)				RMSE(mm/day)				BIAS (%)			
		RTV6_UC	RTV6_C	RTV7_UC	RTV7_C	RTV6_UC	RTV6_C	RTV7_UC	RTV7_C	RTV6_UC	RTV6_C	RTV7_UC	RTV7_C	RTV6_UC	RTV6_C	RTV7_UC	RTV7_C
MAM	US	0.34	0.34	0.35	0.37	-0.01	-0.48	-0.35	-0.31	8.30	7.53	7.44	7.09	-0.60	-20.07	-14.54	-12.94
	East Asia	0.45	0.46	0.47	0.51	-0.91	-0.37	-1.33	-0.57	7.05	8.25	6.78	7.30	-30.81	-12.70	-45.09	-19.47
	Europe	0.36	0.39	0.35	0.38	-0.21	0.59	-0.38	0.19	4.63	5.65	4.46	5.01	-11.53	33.41	-21.63	10.46
	Australia	0.58	0.57	0.60	0.62	-1.11	-0.43	-1.41	-0.50	7.07	7.84	6.87	7.20	-40.68	-15.78	-51.66	-18.24
JJA	US	0.32	0.39	0.38	0.42	0.25	0.21	0.68	0.45	10.24	8.54	9.50	8.25	8.57	7.12	22.79	15.24
	East Asia	0.47	0.51	0.54	0.56	-1.95	0.17	-1.56	0.31	11.56	13.62	10.62	12.16	-35.43	3.16	-28.29	5.70
	Europe	0.42	0.51	0.49	0.51	-0.28	0.57	0.16	-0.11	6.14	6.16	6.23	5.35	-11.00	22.84	6.46	-4.58
	Australia	0.46	0.51	0.55	0.53	-1.32	-0.58	-1.29	-0.68	4.64	5.08	4.39	4.68	-72.68	-31.75	-70.90	-37.36
SON	US	0.34	0.39	0.39	0.41	-0.67	-0.33	-0.69	-0.09	7.26	7.69	6.82	7.76	-27.73	-13.54	-28.40	-3.82
	East Asia	0.40	0.45	0.48	0.51	-1.04	-0.12	-1.08	-0.21	7.76	9.22	7.17	8.12	-39.07	-4.67	-40.86	-7.75
	Europe	0.50	0.54	0.52	0.56	-0.87	0.56	-0.91	0.03	4.90	6.38	4.84	5.55	-36.34	23.39	-37.85	1.02
	Australia	0.57	0.58	0.59	0.61	-0.68	-0.44	-0.92	-0.57	5.77	6.02	5.51	5.55	-28.85	-18.50	-38.71	-24.05
DJF	US	0.30	0.30	0.31	0.31	-0.66	0.01	-0.87	-0.03	5.42	7.59	5.11	6.88	-35.50	0.50	-46.54	-1.66
	East Asia	0.24	0.27	0.28	0.33	-0.70	-0.13	-0.87	-0.41	4.31	5.90	4.08	4.85	-50.13	-9.14	-61.63	-29.24
	Europe	0.33	0.34	0.32	0.34	-1.13	0.39	-1.36	-0.69	4.62	6.95	4.55	5.19	-51.75	17.98	-62.01	-31.59
	Australia	0.63	0.64	0.62	0.65	-0.67	-0.40	-1.35	-0.29	10.67	10.92	10.36	10.60	-13.09	-7.76	-25.49	-5.65
All Seasons	US	0.32	0.36	0.36	0.39	-0.27	-0.15	-0.30	0.01	7.85	8.00	7.39	7.51	-11.26	-6.07	-12.57	0.27
	East Asia	0.45	0.49	0.52	0.54	-1.15	-0.11	-1.21	-0.22	8.10	9.66	7.53	8.52	-36.79	-3.53	-38.63	-6.96
	Europe	0.41	0.46	0.43	0.47	-0.62	0.53	-0.62	-0.15	5.11	6.31	5.07	5.28	-28.07	24.00	-28.09	-6.76
	Australia	0.61	0.61	0.61	0.64	-0.95	-0.46	-1.24	-0.51	7.40	7.80	7.15	7.37	-31.42	-15.31	-41.28	-16.89

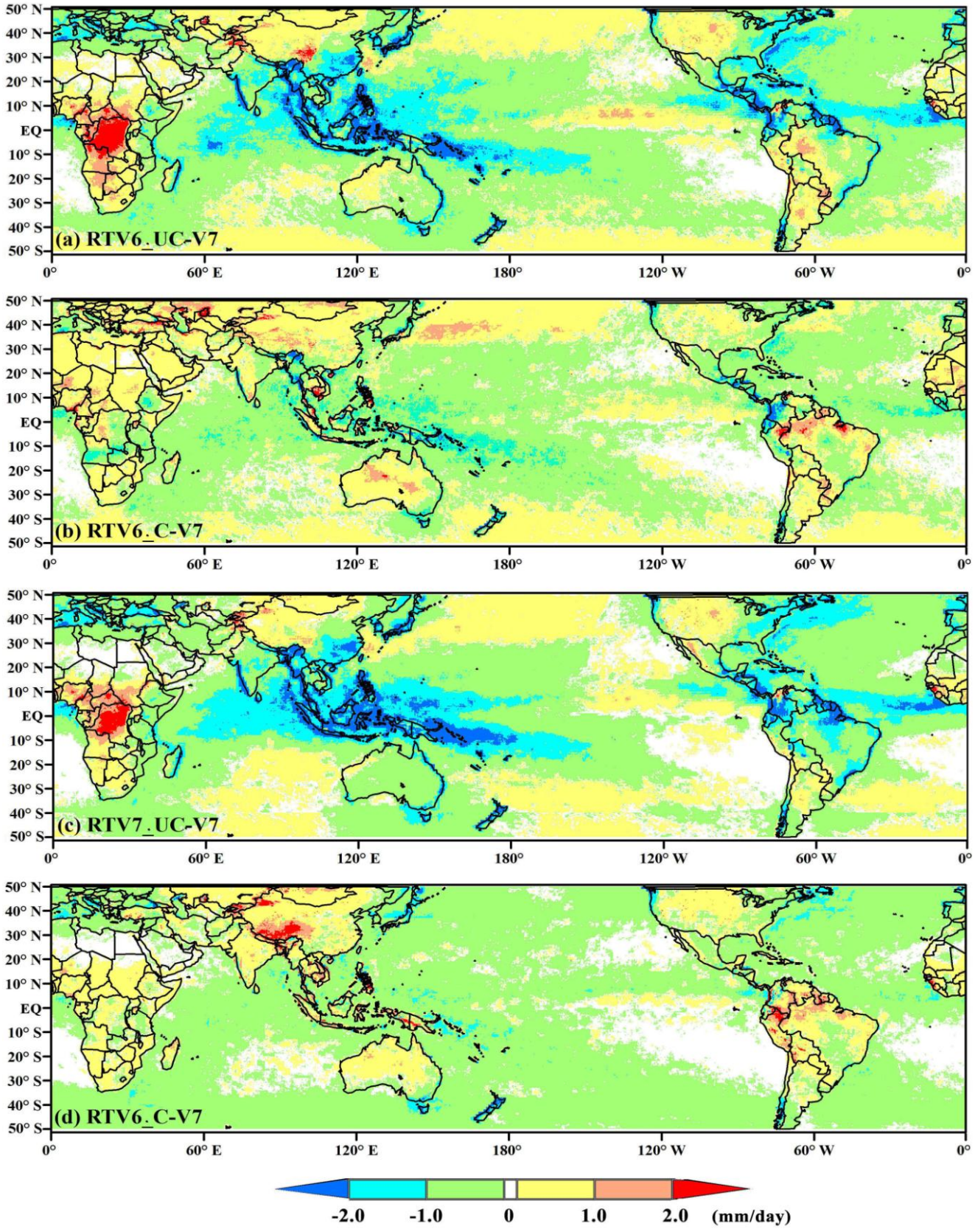
(a) RTV6_UC-V7
(b) RTV6_C-V7
(c) RTV7_UC-V7
(d) RTV6_C-V7
50° N
40° N
30° N
20° N
10° N
EQ
10° S
20° S
30° S
40° S
50° S
0°
60° E
120° E
180°
120° W
60° W
0°
-2.0
-1.0
0
1.0
2.0
(mm/day)

Figure 1. Global map of mean daily precipitation difference between (a) uncalibrated RTV6 data sets (RTV6_UC) and production V7, (b) calibrated RTV6 (RTV6_C) and production V7, (c) uncalibrated RTV7 (RTV7_C) and production V7, (d) calibrated RTV7 (RTV7_C) and production V7 for the three-year study period (from July 2008 to June 2011).

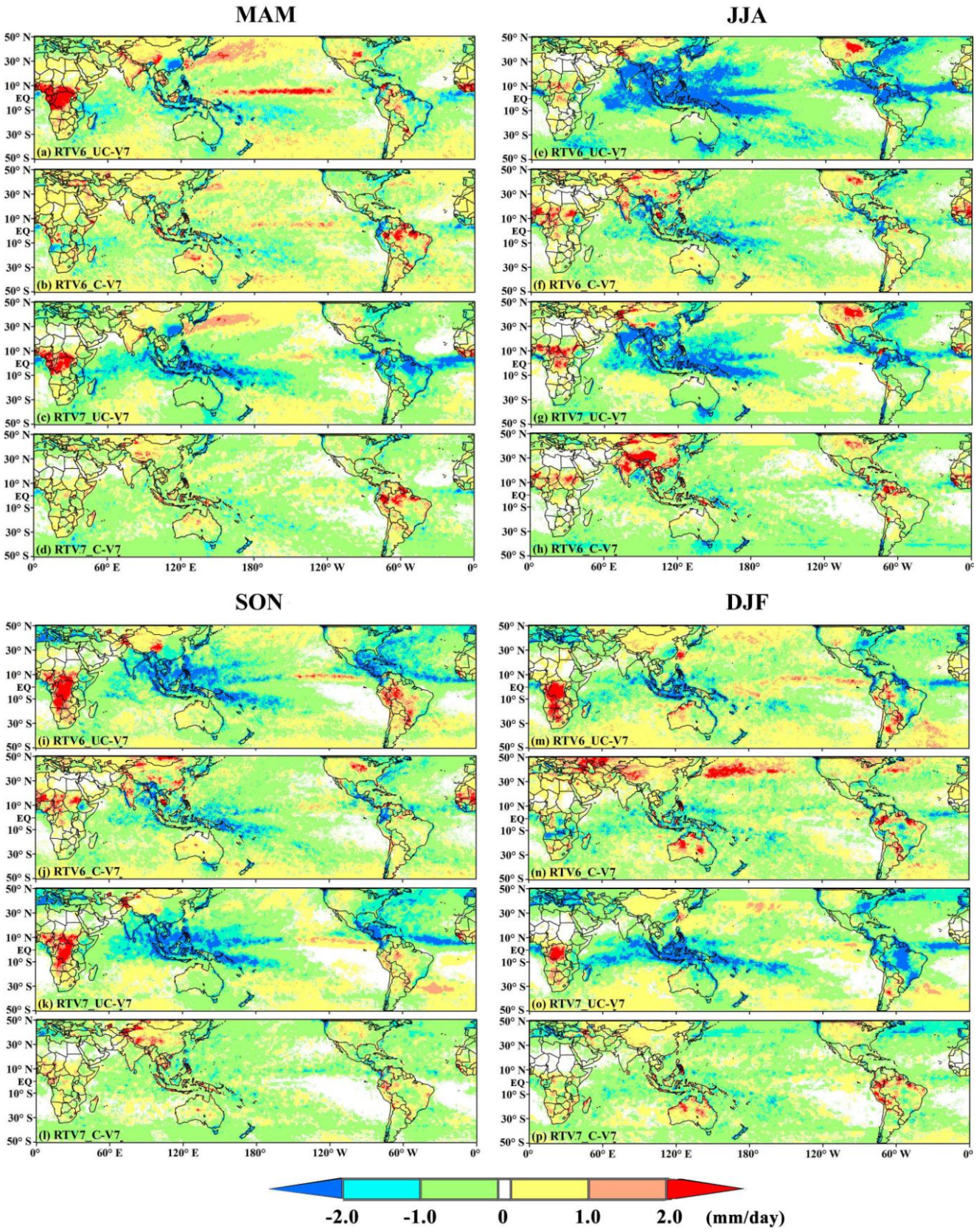
MAM
JJA
SON
DJF
(a) RTV6_UC-V7
(b) RTV6_C-V7
(c) RTV7_UC-V7
(d) RTV7_C-V7
(e) RTV6_UC-V7
(f) RTV6_C-V7
(g) RTV7_UC-V7
(h) RTV6_C-V7
(i) RTV6_UC-V7
(j) RTV6_C-V7
(k) RTV7_UC-V7
(l) RTV7_C-V7
(m) RTV6_UC-V7
(n) RTV6_C-V7
(o) RTV7_UC-V7
(p) RTV7_C-V7
50° N
30° N
10° N
EQ
10° S
30° S
50° S
0°
60° E
120° E
180°
120° W
60° W
-2.0
-1.0
0
1.0
2.0
(mm/day)

545

546 **Figure 2.** As in Fig. 1, but for seasonal variations: boreal (a-d) Spring (March-May), (e-h) Summer
547 (June-August), (i-l) Autumn (September-November), and (m-p) Winter (December-February).

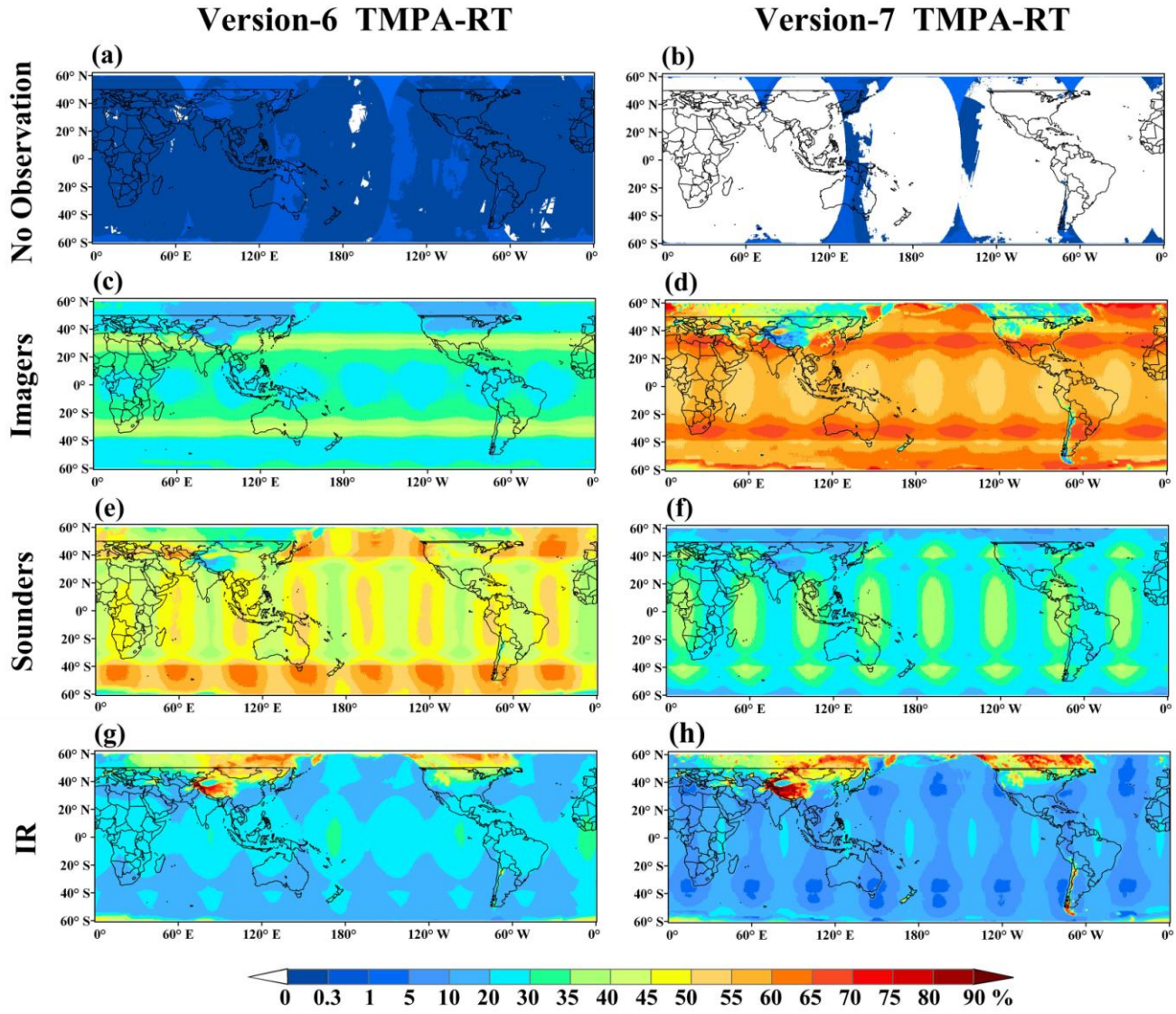

548

549 **Figure 3.** Global distribution of scan frequency of various microwave sensors introduced into the (left

550 column) Version-6 and (right column) Version-7 TMPA real-time system: (a) and (b) No Observation;

551 (c) and (d) Imagers; (e) and (f) Sounders; (g) and (h) IR.

552 **Note:** In the text, the scan frequency of a certain kind of sensors (SF_i) is defined as following:

553 $$SF_i = \frac{SC_i}{SC_{total}} \times 100\% \qquad (1)$$

554 where SC_i is the scan counts of a certain kind of sensors, SC_{total} is the total scan counts for all sensors.

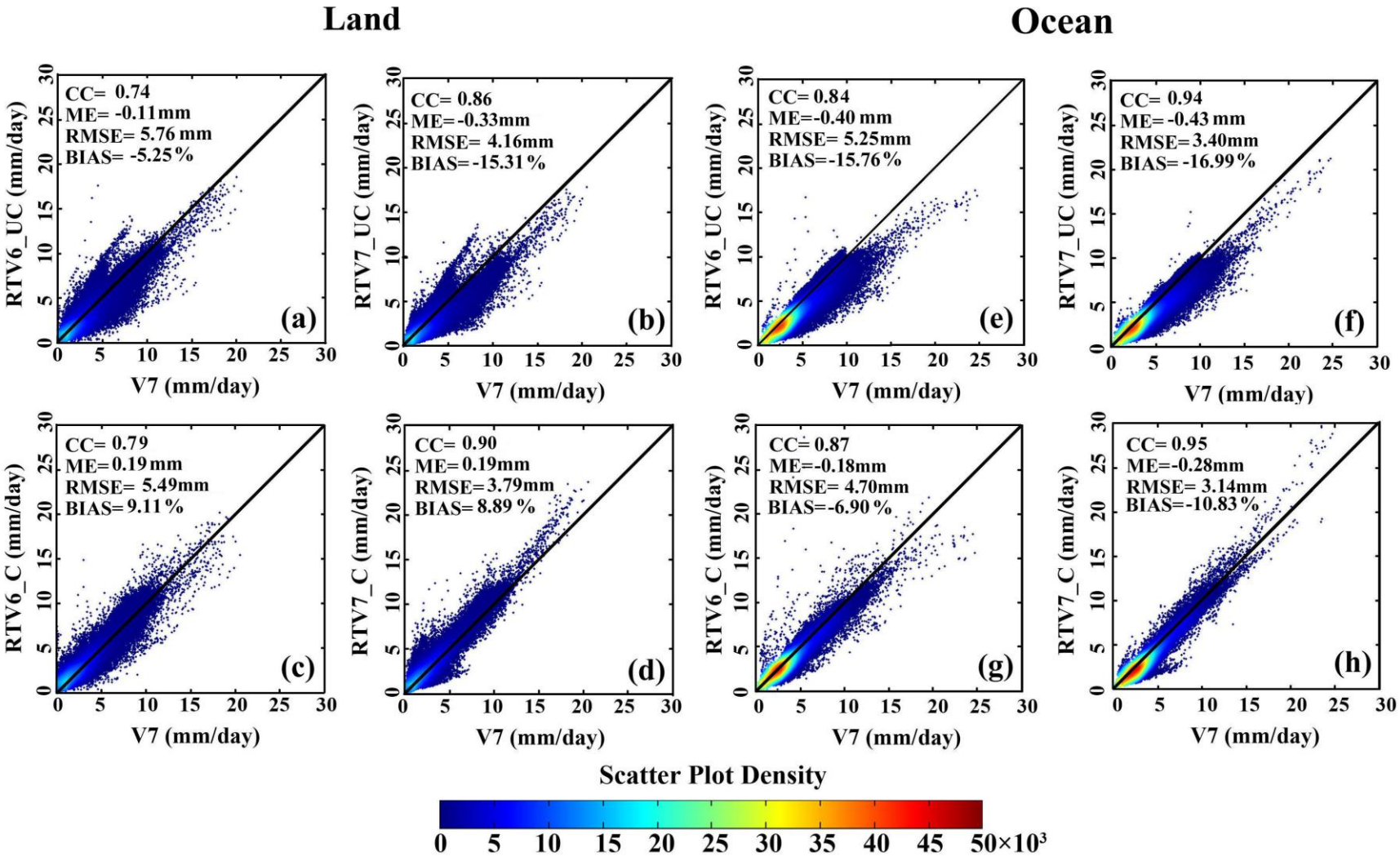

555

556 **Figure 4.** Two-dimensional scatterplots of daily precipitation for (top) uncalibrated and (bottom) calibrated TMPA-RT against

557 production V7 for (left two columns) land and (right two columns) ocean, corresponding to the maps in Fig. 1.

558 **Note:** The formulae and meaning of all statistical indices in each plot are described in more detail in Table 1 of Yong et al. (2010).

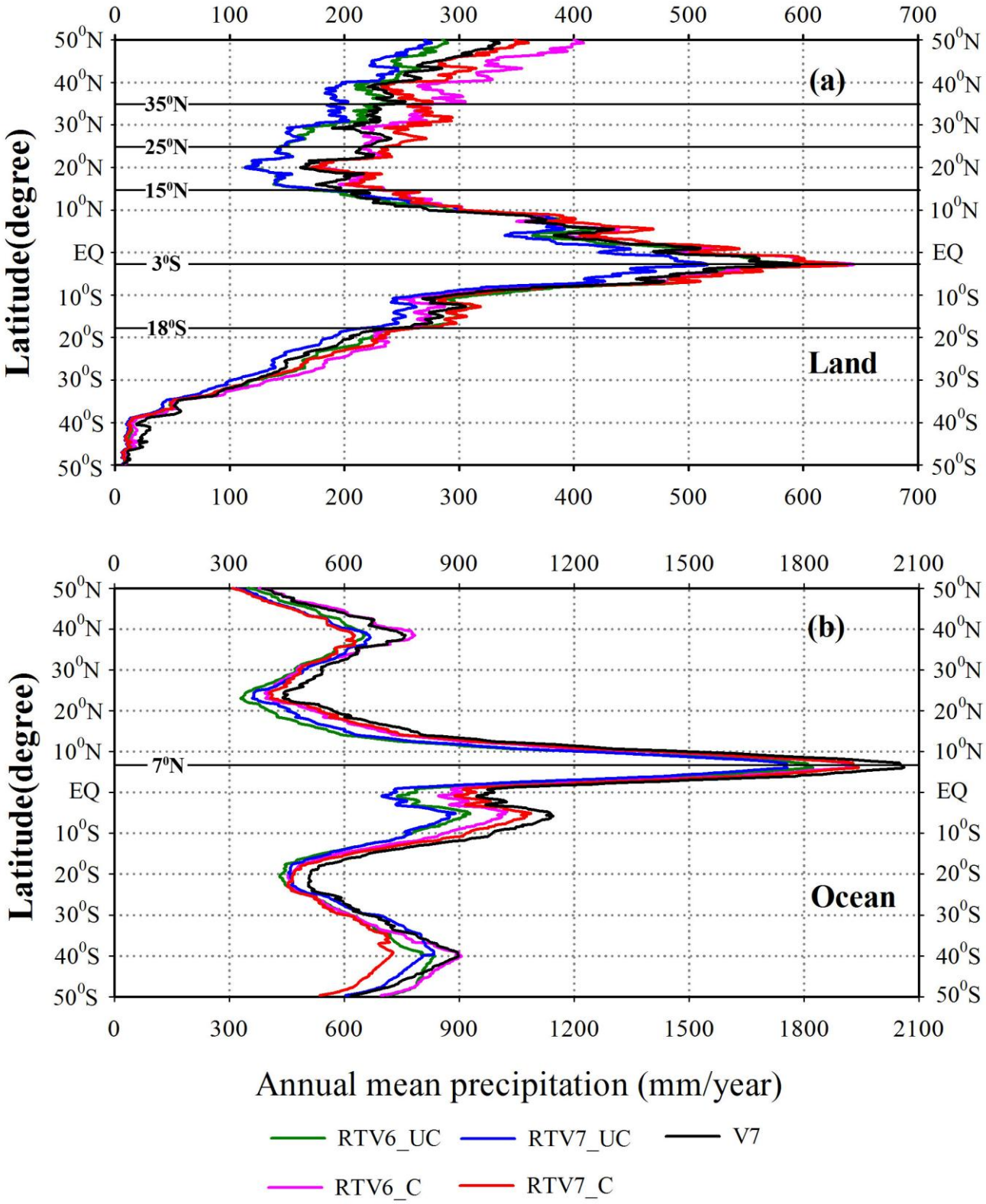

559
560 **Figure 5.** Latitudinal distribution of the annual mean precipitation of four TMPA-RT estimates
561 (RTV6_UC, RTV6_C, RTV7_UC, RTV7_C) and production V7 over both (a) land and (b) ocean.

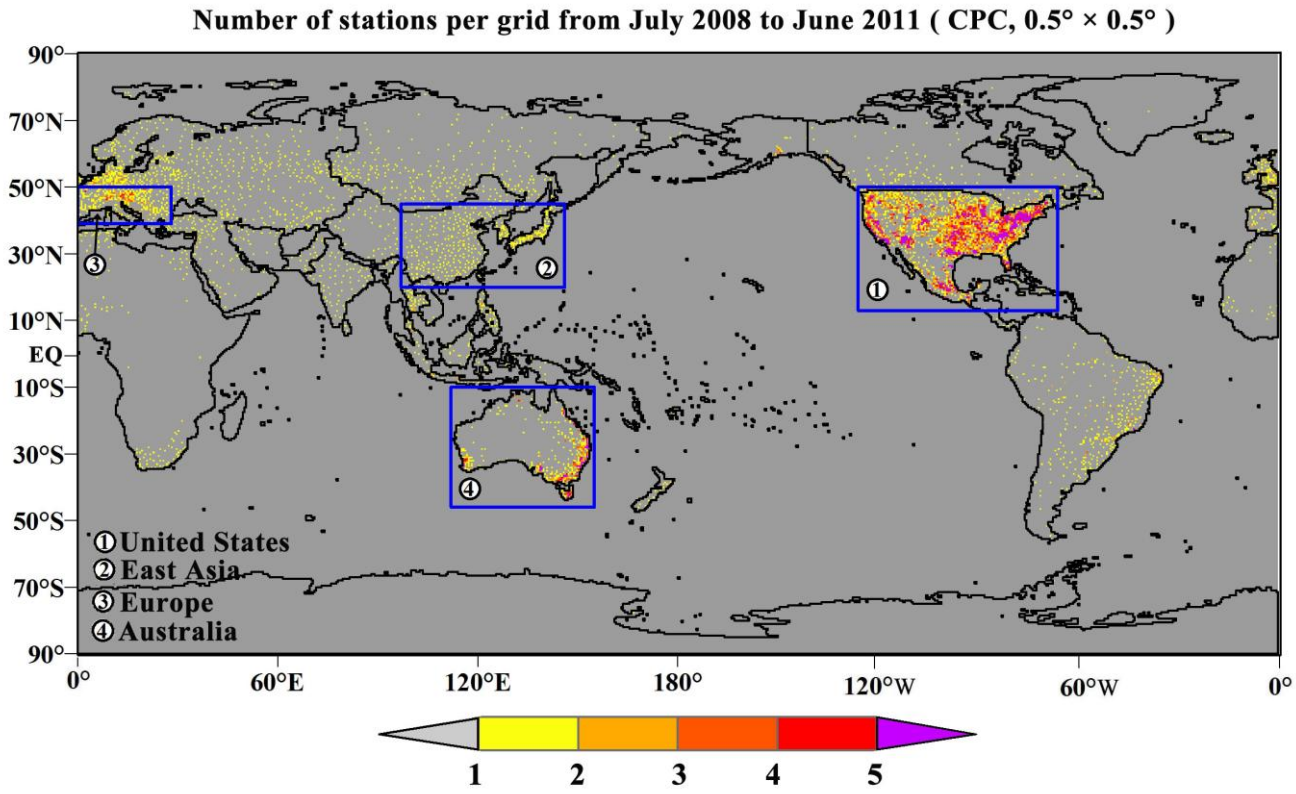

562

563 **Figure 6.** Number of gauge stations in a 0.5° × 0.5° latitude-longitude grid for the CPC unified gauge-
564 based analysis over the global land areas (from July 2008 to June 2011). The four selected validation
565 regions (i.e., United States, East Asia, Europe, and Australia) are also shown.